









RESEARCH ARTICLE | NOVEMBER 18 2024

A scalable, symmetric atom interferometer for infrasound gravitational wave detection

C. Schubert ; D. Schlippert ; M. Gersemann ; S. Abend ; E. Giese ; A. Roura ; W. P. Schleich ; W. Ertmer; E. M. Rasel 

 Check for updates

AVS Quantum Sci. 6, 044404 (2024)

<https://doi.org/10.1116/5.0228398>



View Online



Export Citation

Articles You May Be Interested In

Twenty-four-micrometer-pitch microelectrode array with 6912-channel readout at 12 kHz via highly scalable implementation for high-spatial-resolution mapping of action potentials

Biointerphases (December 2017)

Scalable nanoimprint patterning of thin graphitic oxide sheets and *in situ* reduction

J. Vac. Sci. Technol. B (January 2011)

Scalable multiparty steering using a single entangled photon-pair

AVS Quantum Sci. (June 2024)

18 November 2024 16:36:09




 Advance your science and career as a member of **AVS**

[LEARN MORE >](#)

A scalable, symmetric atom interferometer for infrasound gravitational wave detection



Cite as: AVS Quantum Sci. **6**, 044404 (2024); doi: [10.1116/5.0228398](https://doi.org/10.1116/5.0228398)

Submitted: 12 July 2024 · Accepted: 25 September 2024 ·

Published Online: 18 November 2024



View Online



Export Citation



CrossMark

C. Schubert,^{1,2,a)} D. Schlippert,² M. Gersemann,² S. Abend,² E. Giese,^{2,3} A. Roura,⁴
W. P. Schleich,^{5,6} W. Ertmer,² and E. M. Rase²

AFFILIATIONS

¹German Aerospace Center (DLR), Institute for Satellite Geodesy and Inertial Sensing, Callinstraße 30b, 30167 Hannover, Germany

²Institut für Quantenoptik, Leibniz Universität Hannover, Welfengarten 1, 30167 Hannover, Germany

³Technische Universität Darmstadt, Institut für Angewandte Physik, Schloßgartenstr. 7, 64289 Darmstadt, Germany

⁴German Aerospace Center (DLR), Institute of Quantum Technologies, Wilhelm-Runge-Straße 10, 89081 Ulm, Germany

⁵Institut für Quantenphysik and Center for Integrated Quantum Science and Technology (IQST), Universität Ulm, Albert-Einstein-Allee 11, D-89081 Ulm, Germany

⁶Institute for Quantum Science and Engineering (IQSE), Texas A&M AgriLife Research and Hagler Institute for Advanced Study, Texas A&M University, College Station, Texas 77843-4242, USA

^{a)}Electronic mail: Christian.Schubert@dlr.de

ABSTRACT

We propose a terrestrial detector for gravitational waves with frequencies between 0.3 and 5 Hz based on atom interferometry. As key elements, we discuss two symmetric matter-wave interferometers, the first one with a single loop and the second one featuring a folded triple-loop geometry. The latter eliminates the need for atomic ensembles at femtokelvin energies imposed by the Sagnac effect in other atom interferometric detectors. The folded triple-loop geometry also combines several advantages of current vertical and horizontal matter wave antennas and enhances the scalability in order to achieve a peak strain sensitivity of $2 \times 10^{-21}/\sqrt{\text{Hz}}$.

© 2024 Author(s). All article content, except where otherwise noted, is licensed under a Creative Commons Attribution (CC BY) license (<https://creativecommons.org/licenses/by/4.0/>). <https://doi.org/10.1116/5.0228398>

I. INTRODUCTION

The direct observation of gravitational waves with laser interferometers^{1,2} marks the beginning of a new area in astronomy with new searches targeting signals in a broader frequency band with a variety of detectors. One class of proposed detectors relies on atom interferometers rather than on macroscopic mirrors as inertial references. Indeed, both vertical^{3–10} or horizontal^{10–12} baselines interrogated by common laser beams propagating along those baselines have been proposed for terrestrial observatories.¹³ In this article, we present a new class of symmetric atom interferometers enabling single and multi-loop^{14–16} geometries for broad- and narrow-band detection in the frequency range¹⁷ of 0.3–5 Hz.

Today's detectors are based on laser interferometers and operate in the acoustic frequency band between ten and hundreds of hertz.^{1,2,18,19} Future space-borne interferometers, such as LISA,^{20–24} are designed to target signals in the range of millihertz to dechihertz. Detectors operating in the mid-frequency band^{25–27} or improving on

the frequency band of current ground-based devices^{28,29} have also been proposed and investigated. Moreover, recent results from pulsar timing arrays indicate the existence of a signal at ultralow frequencies.^{15,30–33}

After first suggestions exploiting mechanical resonators^{34–36} and atomic spectroscopy such as hole burning,^{37–40} matter-wave interferometers,^{3,4,6,11,12,41–47} and optical clocks⁴⁸ are pursued to search for sources of gravitational waves in the infrasound domain featuring frequencies inaccessible for today's ground-based detectors. Waves in this band are emitted, for example, by inspiraling stellar-mass binaries days or hours before they merge within fractions of a second^{49,50} as the first observed event GW150914,^{1,2} but also by inspirals around an intermediate-mass black hole or mergers of two intermediate-mass black holes, which never emit significantly in the Advanced LIGO band.^{13,17} Hence, atom-interferometric observation in the infrasound band could be combined with standard astronomical observations for improved angular localization and prediction of upcoming events for

other detectors.⁵¹ The vast benefits of joint observations manifested itself in the case of a merger of neutron stars.⁵²

Our proposed detector is based on a type of interferometer where matter waves form a single or several folded loops of symmetric shape.⁵³ Compared to single-loop interferometers, dual- or triple-loop geometries suppress dependencies on input parameters.^{11,46,54,55} While a folded double-loop interferometer is also possible,^{56,57} we choose a folded triple-loop scheme as the study case of this paper due to its inherent features.

An antenna employing folded multi-loop interferometers shows three distinct advantages: (i) The detector is less susceptible to environmental perturbations, and less restrictive on the expansion rate of the atomic ensemble, which otherwise needs to be at the energy level of femtokelvins. (ii) It combines the scalability of arm lengths of horizontal and the single-laser link of vertical antenna types, (iii) and it is less susceptible to technical noise such as the pointing jitter of the atomic sources.

In this article, we explain the concept of our detector and compare a symmetric single-loop interferometer with a folded multi-loop one, confronting their scaling, spectral responses, and critical parameters. Similar to the matter-wave interferometric gravitational antenna MIGA^{12,58,59} and laser interferometers,^{1,2} our detector concepts have two perpendicular, horizontal arms, depicted in Fig. 1(a), suppressing laser frequency noise at lower frequencies as in light interferometers.^{1,18,21} Two light-pulse atom interferometers, separated by a distance L , and located in each arm, are sensitive to the phase of the light pulses traveling along the x and y axes between the interferometers and are employed for coherent manipulation of the atoms. A gravitational wave, propagating along the z axis, modifies the geodesic of the light connecting the interferometers and modulates its phase which appears in the differential signal of the two atom interferometers.

Our article is organized as follows: in Sec. II, we introduce the symmetric single-loop geometry of our gravitational wave detector based on atom interferometry. Although this arrangement is in principle sensitive to gravitational waves, the need to suppress the spurious Sagnac effect enforces kinetic expansion energies of the atomic ensemble beyond reach. For this reason, we propose in Sec. III the multi-loop geometry and discuss in great detail in Sec. IV the necessary experimental requirements. We conclude by summarizing our results in Sec. V.

In order to focus on the essential points but, at the same time, keep our article self-contained, we have included detailed discussions in four Appendixes. In Appendix A, we estimate the parameters for the twin lattice used to re-launch the atoms. Appendix B is dedicated to a brief analysis of the influence of timing errors on the coherent re-launch. Finally, requirements on the parameters specifying the single-loop and the triple-loop are discussed in Appendixes C and D, respectively.

II. SYMMETRIC SINGLE-LOOP GEOMETRY

In contrast to other approaches,^{6,59} our atom interferometers are symmetric^{46,60–62} as an identical number of photon recoils is transferred to both paths of the atom interferometer during beam splitting, deflection, and recombination. For this purpose, we employ a twin-lattice, i.e., two counter-propagating lattices formed by retroreflecting a light beam with two frequency components. To the lowest order, such a double-diffraction scheme^{62,63} suppresses laser phase noise, inherently doubles the momentum transfer entering the scale factor of the interferometer, suppresses error terms similarly to k -reversal

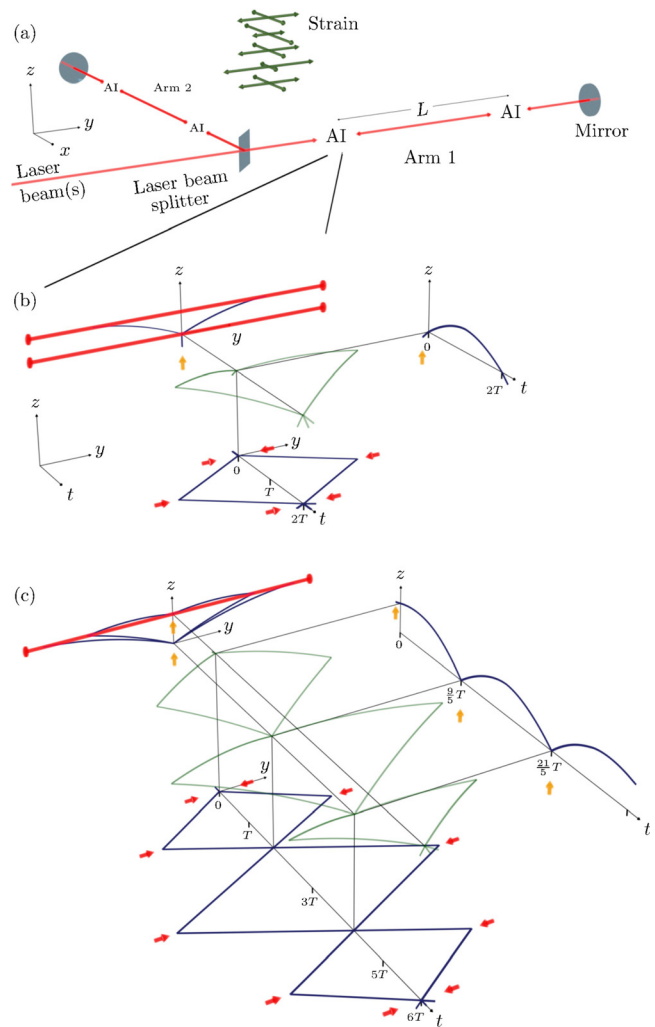


Fig. 1. (a) Matter-wave detector for infrasound gravitational waves. Two horizontal arms (along x and y) each with two atom interferometers are sensitive to the phase of the light beams (red lines). The detector is maximally sensitive to gravitational waves traveling along z , and periodically stretching and squeezing the detector arms. (b) Spacetime diagram and geometric projections of a symmetric single-loop atom interferometer with a pulsed twin-lattice formed by retroreflection. Atoms are launched vertically along z [orange arrows in the $z(y)$ and $z(t)$ diagrams] by a coherence preserving mechanism such as Bloch oscillations combined with double Bragg diffraction (Ref. 70). The first interaction with the bottom twin-lattice at $t=0$ excites the atoms into a coherent superposition of two opposite momenta as shown in the $z(y)$ and $y(t)$ diagrams. The second interaction at the apex at $t=T$ inverts the momenta and, finally, a recombination pulse at the bottom lattice at $t=2T$ enables interference. (c) After exciting the atoms into a coherent superposition of two momenta at $t=0$, three subsequent interactions each inverting the momenta at $t=T, t=3T, t=5T$, form three loops before the recombination at $t=6T$. The two vertical relaunches at $t=(9/5)T$ and $t=(21/5)T$ fold the interferometer geometry which requires only a single horizontal beam splitting axis for manipulating the atoms as opposed to (b).

techniques,⁶⁴ and can be combined with large-momentum-transfer techniques.⁶⁰ We expect these advantages to outweigh the subtleties^{61,65,66} associated with its implementation, such as the limited flexibility for chipping,⁶⁷ the emergence of spurious paths,⁶⁸ and its

susceptibility to polarization errors.⁶⁹ Neglecting the non-vanishing pulse duration of the atom–light interaction,^{71–74} the phase difference^{6,47} in the single-loop atom interferometer of Fig. 1(b) induced by a gravitational wave of amplitude h and angular frequency $\omega \equiv 2\pi f$ reads

$$\phi_{\text{SL}} = 2hkL[\cos(2\pi fT) - 1]. \quad (1)$$

Hence, three parameters determine the spectral sensitivity of such a detector: (i) The distance L between the interferometers, (ii) the number of photon momenta transferred differentially between the two interferometer paths corresponding to the wave number k , and (iii) the pulse-separation time T . The ability to change T in this setup allows for adjusting the frequency of the maximum spectral response which scales with the inverse of T .

Unfortunately, spurious effects can mask the phase induced by a gravitational wave. For example, in the single-loop interferometer, the shot-to-shot jitter of the initial velocity \mathbf{v} and position \mathbf{r} causes noise as it enters the phase terms^{75,76} $2(\mathbf{k} \times \mathbf{v}) \cdot \boldsymbol{\Omega}T^2$, $\mathbf{k} \cdot \boldsymbol{\Gamma} \mathbf{r}T^2$, and $\mathbf{k} \cdot \boldsymbol{\Gamma} \mathbf{v}T^3$ arising from the Sagnac effect and gravity gradients. Here, $\boldsymbol{\Omega}$ and $\boldsymbol{\Gamma}$ denote Earth’s angular velocity and the gravity gradient tensor, respectively.⁷⁷

Whereas the impact of gravity gradients can be compensated,^{78,79} typical parameters targeting a competitive strain sensitivity enforce kinetic expansion energies of the atomic ensembles to suppress the spurious Sagnac effect corresponding to femtokelvin temperatures. Such a regime is beyond reach even with delta-kick collimation.^{80–83}

III. SYMMETRIC MULTI-LOOP GEOMETRY

This challenge can be mitigated by a suitably tailored geometry with atomic trajectories following multiple loops inside the interferometer^{46,84} as depicted in Fig. 1(c). In this scheme, the interferometer begins after a vertical launch at time $t = 0$, with the first interaction with the symmetric twin lattice creating a coherent superposition of two momentum states. Subsequently, the atoms are coherently reflected at $t = T$ along the horizontal direction so that they complete their first loop and the paths of the atom interferometer corresponding to the trajectories of the two partial atomic wave functions intersect at the bottom at $t = (9/5)T$. Here, they are launched upwards again,⁷⁰ and their horizontal motion is inverted at the vertex in the middle of the interferometer at $t = 3T$. After completion of the second loop, they are again relaunched at $t = (21/5)T$, once more redirected at $t = 5T$, and finally recombined at $t = 6T$ to close the interferometer.

In order to suppress spurious phase contributions due to the Sagnac effect and gravity gradients, the wave numbers of the five pulses are adjusted⁴⁶ to k , $\frac{9}{4}k$, $\frac{5}{2}k$, $\frac{9}{4}k$, k , corresponding to the differential momentum between the two paths of the interferometer.

Compared to the symmetric single-loop interferometer, the adjusted wave numbers and additional loops change the phase difference between the two interferometers⁴⁶ which now reads

$$\phi_{\text{FTL}} = \frac{1}{2}hkL[5 - 9\cos(2 \cdot 2\pi fT) + 4\cos(3 \cdot 2\pi fT)], \quad (2)$$

for our folded triple-loop sequence.

This scheme shares the advantage of a horizontal detector^{12,59} enabling us to operate the interferometers separated by up to several ten kilometers similar to light interferometers.^{1,2} Moreover, it requires only a *single* horizontal beam axis in each arm for the coherent

manipulation of the atoms. Here, T can be tuned to specific frequencies of the gravitational waves¹⁴ similar to vertical antennas, where the light beam propagates along the direction of the free fall of the atoms. This feature differs from the configuration with two horizontal beams, in which the height difference between them constrains T .

IV. PARAMETER REQUIREMENTS AND STRAIN SENSITIVITY

The folded triple-loop interferometer mitigates several important drawbacks of other concepts. For example, the specific combination of three loops and increased momentum transfer by the central pulses compared to the initial and final pulse renders this interferometer insensitive to fluctuations of initial position and velocity,⁴⁶ mitigating the requirement for femtokelvin energies.

Unfortunately, folded multi-loop interferometers are susceptible to pointing noise of the relaunch vector. In a model with a vanishing atom–light interaction time and no timing errors, the requirements remain comparable to those for a single-loop geometry and have to be limited to picoradians. For relaunches not centered on the intersections of the trajectories, see Fig. 1(c), new terms appear if their directions are not properly aligned. See Appendix B for the impact of timing errors. Table I summarizes the requirements imposed by the two geometries. Mean-field effects constrain the initial density and consequently the size of the atomic ensemble for a given number of atoms.^{6,85} In the single-loop scheme, these constraints introduce requirements on the beam-splitting fidelity and gravity-gradient compensation⁷⁹ to avoid other phase errors linked to large size. However, they are relaxed in the multi-loop scheme as briefly discussed in Appendix D.

Figure 2 compares the spectral strain sensitivities, obtained by the broad-band mode of the single- (green lines) and triple-loop detector (red lines), and the narrow-band mode (cyan lines) of the multi-loop geometry, with a signal (orange dashed-dotted line) generated by a black hole binary.⁴⁹ They are also confronted with the anticipated strain sensitivity of the space-borne detector LISA²¹ (black dotted line) and the operating advanced LIGO^{86,87} (brown dashed-dotted line). We emphasize that the sensitivity curves of our detector concepts fill the gap between LISA and advanced LIGO, enabling the terrestrial detection of infrasound gravitational waves. To put our proposed scheme into the context of adjacent frequency bands and third-generation optical gravitational wave detectors, we present in Appendix E the strain sensitivity over a broader range of frequencies including a rough estimate for the Einstein Telescope.²⁹

With respect to the strain sensitivity, our designs share assumptions with other proposals^{12,59} based on atom interferometry. For two 10-km-long arms, we foresee an intrinsic total phase noise of $1 \mu\text{rad}/\sqrt{\text{Hz}}$ achieved by 10^9 atoms starting every 100 ms with an upward velocity of $gT/2$, where g is the gravitational acceleration. Moreover, we expect 20 dB sub-shot-noise detection,⁸⁸ a maximum of $T \sim 260$ ms, and the symmetric transfer of 1000 photon recoils at the rubidium D2 line in each direction, see Appendix A for parameter estimates.^{60,89–96}

Recent research addresses relevant building blocks for the presented geometry: the anticipated high launch and beam-splitting efficiencies during large momentum transfer are expected to benefit^{60,70,97–100} from delta-kick collimated ensembles of rubidium⁸¹ and Bose–Einstein condensates^{80,82,83} which feature residual atomic expansion rates of less than $100 \mu\text{m/s}$, corresponding to ~ 100 pK for

TABLE I. Order-of-magnitude requirements on key parameters of the atomic source and launch mechanisms for the single-loop and triple-loop interferometer. Here, we list only the dominant contributions originating from the terrestrial gravity gradient and the Sagnac effect. The instabilities in position δy and velocity δv_x , δv_y refer to 1 s operation time which corresponds to ten interferometry cycles. Similarly, the both gravity gradients and Sagnac effect pose requirements on the pointing for the relaunch pulses $\delta\alpha_x$, $\delta\alpha_y$, and $\delta\alpha_{v,x}$. We assume a maximum phase noise of $\sigma\phi = 1 \mu\text{rad}$ in 1 s with $k = 2000 \cdot 2\pi/(780 \text{ nm})$, and $T = 0.26 \text{ s}$. Typical values for gravity gradients, the Earth rotation, and the gravitational acceleration are $\Gamma = 1.5 \times 10^{-6} \text{ s}^{-2}$, $\Omega = 5.75 \times 10^{-5} \text{ rad/s}$, and $g = 9.81 \text{ m/s}^2$, respectively. The vertical distance between source and beam splitting zone is $l = 30 \text{ cm}$. The requirements on the pointing of the diffraction beam, assuming an uncertainty $\delta g/g = 10^{-7}$ in the linear acceleration, is given by $\delta\beta$. Requirements on the relative relaunch pointing refers to an instability in the angle between the relaunch at $t = (9/5)T$ and $t = (21/5)T$. A jitter in the pointing leads to a coupling to Γ and Ω . The latter one, denoted by $\Delta\alpha_x$, dominates for our choice of parameters. The values in the upper part of the table (from δy to $\Delta\alpha_x$) assume no timing error for the relaunch. The pointing constraint $\Delta\alpha$ set by a timing error shifting the relaunches by $\Sigma_\tau = 10 \text{ ns}$ is shown at the bottom. Experiments have demonstrated (Refs. 80 and 83) standard deviations of the mean velocity of the atomic ensemble below $100 \mu\text{m/s}$, significantly below the requirements for the triple-loop geometry set in the table.

	Single-loop	Triple-loop
δy	$\sim \frac{\sigma\phi}{k\Gamma T^2} \sim 10^{-10} \text{ m}$	$\sim \frac{\sigma\phi}{k\Gamma^2 T^4} \sim 10^{-3} \text{ m}$
δv_y	$\sim \frac{\sigma\phi}{k\Gamma T^3} \sim 10^{-9} \text{ m/s}$	$\sim \frac{\sigma\phi}{k\Gamma^2 T^5} \sim 10^{-2} \text{ m/s}$
δv_x	$\sim \frac{\sigma\phi}{k\Omega T^2} \sim 10^{-11} \text{ m/s}$	$\sim \frac{\sigma\phi}{k\Omega^3 T^4} \sim 10^{-2} \text{ m/s}$
$\delta\alpha_y$	$\sim \frac{\sigma\phi}{lk\Gamma T^2} \sim 10^{-9} \text{ rad}$	$\sim \frac{\sigma\phi}{lk\Gamma^2 T^4} \sim 10^{-2} \text{ rad}$
$\delta\alpha_{v,y}$	$\sim \frac{\sigma\phi}{kgT^2\Gamma T^2} \sim 10^{-10} \text{ rad}$	$\sim \frac{\sigma\phi}{kgT^2\Gamma^2 T^4} \sim 10^{-3} \text{ rad}$
$\delta\alpha_{v,x}$	$\sim \frac{\sigma\phi}{kgT^2\Omega T} \sim 10^{-12} \text{ rad}$	$\sim \frac{\sigma\phi}{kgT^2\Omega^3 T^3} \sim 10^{-2} \text{ rad}$
$\delta\beta$	$\sim \frac{\sigma\phi}{k\delta g T^2} \sim 10^{-10} \text{ rad}$	$\sim \frac{\sigma\phi}{k\delta g T^2} \sim 10^{-10} \text{ rad}$
$\Delta\alpha_x$	n/a	$\sim \frac{\sigma\phi}{kgT^2\Omega T} \sim 10^{-12} \text{ rad}$
$\Delta\alpha$	n/a	$\sim \frac{\sigma\phi}{kgT\Sigma_\tau} \sim 10^{-9} \text{ rad}$

^{87}Rb . Additionally, such expansion rates enable ensemble sizes of about $500 \mu\text{m}$ after 1.6 s total time of flight in broad-band mode or $1100 \mu\text{m}$ after 4.7 s total time of flight in resonant mode to ease constraints on the beam diameters for coherent manipulation and the detection process. Relaunches¹⁰¹ can be implemented by two counter-propagating light fields injected from different optical ports^{102–104} or two retro-reflected light fields injected from the same optical fiber port.⁷⁰ In the latter case, the relative pointing of the relaunch vector is coupled to the orientation of the retro-reflection mirror, which can be placed on a dedicated isolation system to suppress pointing noise. Moreover, these implementations can be combined with techniques that tailor individual light pulses and enhance their efficiency even further. Such methods of an optimal control theory potentially relax the constraints on the longitudinal atomic momentum distribution, the expansion rate of the atomic cloud, and uncompensated vibrational

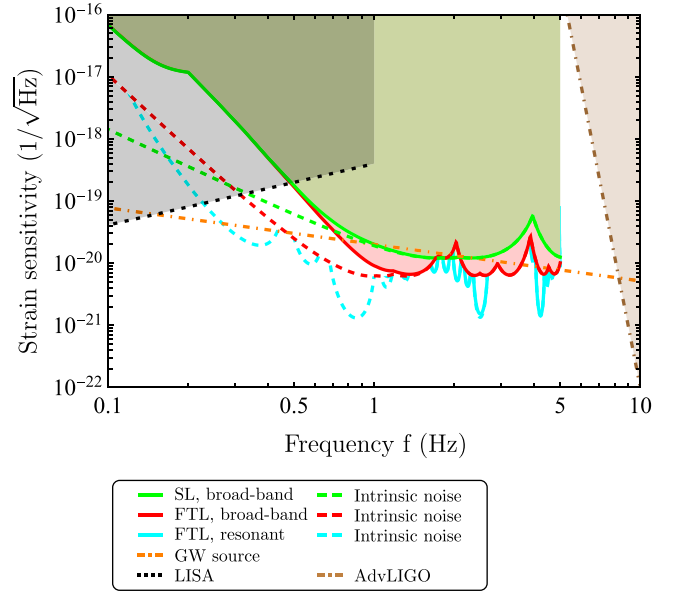


Fig. 2. Spectral strain sensitivities of symmetric single (green lines) and multi-loop (red lines) interferometer compared to the strain induced by a black hole binary (Ref. 49) (orange dashed-dotted line), including sky as well as polarization averaging (Ref. 87). Solid lines illustrate the effective detector sensitivity including vibrations of the retroreflection mirrors and Newtonian noise (Ref. 59) assuming the isolation system from VIRGO (Ref. 117). In the broad-band mode, both reach an intrinsic sensitivity (green dashed line, red dashed line) of better than $10^{-19} / \sqrt{\text{Hz}}$ between 0.3 and 5 Hz running three interferometer sequences interleaved with different free-evolution times T (182, 234, 260 ms). The triple-loop can be extended to a resonant mode by increasing the number of atomic loops leading ideally to a higher intrinsic sensitivity at specific frequencies determined by T . The nine-loop interferometer for $T = 260 \text{ ms}$ is about three times more sensitive at 0.85 Hz (cyan dashed line, only shown if lying below the red or red dashed line). The spectral response of our detectors fills the gap between the space-born detector LISA (Ref. 21) (black dotted line) and advanced LIGO (Refs. 86 and 87) (brown dashed-dotted line).

noise. They have already proven successful in the development of advanced and robust atom-interferometer pulses, primarily in the context of single Bragg diffraction,^{100,105–107} but have recently been extended to double Bragg diffraction schemes.⁶⁹ Combining those methods with Bose–Einstein condensates is compatible^{108,109} with the future utilization of entangled atoms.^{110,111}

In addition, the assumed production rate of atomic ensembles enables an interleaved^{112,113} operation of several interferometers. Indeed, for the broad-band mode, we employ for the single- and triple-loop detector three interleaved interferometers with the free-fall times $T_1 = T$, $T_2 = 0.9T$, and $T_3 = 0.7T$ to avoid peaks in the transfer function⁴³ resulting in the depicted intrinsic strain sensitivities (green, red dashed line). To prevent a temporal or spatial overlap of the atom–light interaction of the individual interferometers and thus to avoid crosstalk, the duration of each interaction is assumed to be less than 6 ms for the chosen parameter set. This choice is consistent with the achieved symmetrical transfer of 1008 photon recoils in less than 4 ms.¹¹⁴

Moreover, we extend the triple-loop scheme to a narrow-band mode¹⁴ featuring $3n$ loops, with a sensitivity enhanced by a factor

$n \in \mathbb{N}$ at a specific frequency determined by the free-fall time T . This resonant-mode detection comes at the cost of an decreased bandwidth and an increase in the overall duration $6nT$ of the interferometer that obviously must not exceed the duration of the signal in the aimed frequency band and must still allow for sufficient integration time. In addition, scaling up the overall duration of the interferometer will also cause problems due to dilute atomic ensembles with large spatial extend. Moreover, T is limited by the vertical height of the chamber and the spatial separation of the atom–light interaction regions, in contrast to vertical setups, where increasing n reduces the available baseline.¹⁵ The cyan line in Fig. 2 shows the sensitivity for the frequency 0.85 Hz, corresponding to $T = 260$ ms, and $n = 3$. According to the Nyquist theorem,¹¹⁵ the interleaved operation with a cycle frequency of 10 Hz implies a high-frequency cut-off at 5 Hz. This cycle frequency assumes a preparation time of 100 ms, for which we anticipate the combination of multiple sources¹¹⁶ or subsequently launching a fraction of an atomic samples. For this set of parameters, the overall duration of one interferometer is 1.6 s. An event in the aimed detection band of 0.85 Hz persists⁴⁹ for 3600 s. Aiming, e.g., for ten data points during that observation time implies a maximum interferometer time of $6nT \leq 360$ s, implying $n \leq 240$. Technical constraints will likely imply a lower limit. They may be linked to losses during the beam splitting operations and thereby implicitly to the ensemble size at the end of the interferometer or explicitly to the final-size requirements for an efficient detection of the interferometer output ports. Here, a choice of $6nT \cdot 100 \mu\text{m/s} \leq 1$ cm as maximum ensemble size¹⁰³ corresponds to $n = 30$.

Next to atomic shot noise, other technical and environmental noise sources¹¹⁸ deteriorate the strain sensitivity. Their impact is evaluated by the transfer function⁷³ of the interferometers. Figure 2 shows that the intrinsic strain sensitivity of the single-loop⁵⁹ (SL, green dashed line) and folded triple-loop (FTL, red dashed line) interferometer decays with f^{-2} and f^{-4} at lower frequencies. Below 1 Hz, vibration models^{59,119,120} of the retroreflecting mirrors and Newtonian noise lead to a limitation of the strain sensitivity (green, red, cyan solid lines). The implementation of several, specifically spaced pairs of atom interferometers in each arm, combined with our proposed geometry, may allow for the suppression of Newtonian noise⁵⁹ (see also Appendix E), which limits the sensitivity at low frequencies. Mirror vibrations enter in the differential signal of the interferometers due to the finite speed c of light causing a delay of $2L/c \approx 70 \mu\text{s}$ and are modeled with a differential weighting function.⁷³ A suspension system isolating the retro-reflection mirror^{117,121} against seismic noise⁵⁹ reduces this contribution to a level similar to the Newtonian noise.

We emphasize that the spectral sensitivity, in particular, the low-frequency cut-off, can be tuned by the free-fall time T of the atoms. In the case of the triple-loop interferometer, the maximum value of T is only determined by the free-fall height. For example, in a ~ 1 m-high chamber T can be tuned up to 260 ms.

In contrast, in the single-loop interferometer, the tuning capability is restricted by the separation of the two twin lattices as illustrated in Fig. 1(b). With $T = 260$ ms and adding 12 ms for beam splitting, a height difference of 37 cm is needed. In our scenario, the triple-loop detector surpasses the signal-to-noise ratio of the single-loop by a factor of about 2 for the broad-band, and about 9 for the narrow-band mode.

The relaunches introduce additional noise terms to the folded triple-loop interferometer. See Appendix B for a discussion of the error

due to imperfect pointing and timing as well as the approach to adjust the absolute pointing with the interferometer itself. Implementations at the most quiet sites, featuring a residual rotation noise¹²² of 2×10^{-11} (rad/s)/ $\sqrt{\text{Hz}}$ enforce either measures such as mechanical noise dampening by one order of magnitude, or atom interferometric measurements sharing a relaunch pulse for two interleaved cycles^{112,113,123,124} to comply with the requirement on pointing noise. Having the second relaunch of the first cycle as the first of a subsequent one leads to a behavior of $\sim 1/t$ for an integration time t . For a white pointing noise, assuming a normal distribution with $\sigma = 2 \times 10^{-11}$ rad at 1 s, the limit set by the intrinsic noise would be reached after an integration time of 400 s. As an example, GW150914 spent approximately 1400 s to chirp from 0.9 to 1.1 Hz,⁴⁹ thus allowing for sufficient integration time to reach the intrinsic noise.

V. CONCLUSION AND OUTLOOK

To summarize, present designs of terrestrial detectors of infrasound gravitational waves based on atom interferometry face several major challenges related to scalability and atomic expansion often necessitating femtokelvin temperatures. Therefore, we propose atomic folded-loop interferometers for horizontal antennas, which overcome these stringent requirements at the cost of a very stable relaunch of the atoms.

The presented approaches are benefiting from symmetric manipulation of the atomic ensemble in which identical amounts of photon recoils are transferred along both interferometer paths. The schemes studied in this article take the form of either symmetric single or multi-loop geometries. In particular, the folded triple loop interferometer has the advantage that it is insensitive to fluctuations in the atomic initial position and velocity due to a cancelation of Sagnac phases by a suitable choice of transferred momenta. In addition, they also combine the advantages of horizontal detectors and vertical setups. As horizontal antennas, they display a scalability of the arm length, and do not rely on deep shafts. Furthermore, the tunability of the spectral response of vertical detectors is maintained, especially the low-frequency cutoff, so that broadband and resonant detection modes are possible. Combining our proposed scheme with techniques that suppress the strict limitations given by Newtonian noise through correlated interferometer arrays⁵⁹ opens a new pathway to reach strain sensitivities of the order of $7 \times 10^{-21}/\sqrt{\text{Hz}}$ at 1 Hz in terrestrial detectors.

ACKNOWLEDGMENTS

The authors thank Víctor J. Martínez-Lahuerta for valuable and fruitful discussions. This work is supported by “Niedersächsisches Vorab” through the “Quantum- and Nano-Metrology (QUANOMET)” initiative within Project No. QT3, the CRC 1227 DQmat within Project Nos. B07 and B09, the CRC 1128 geo-Q within the project A02, the QUEST-LFS, the Deutsche Forschungsgemeinschaft (DFG, German Research Foundation) under Germany’s Excellence Strategy—EXC-2123-B2, and the German Space Agency at the German Aerospace Center (Deutsche Raumfahrtagentur im Deutschen Zentrum für Luft- und Raumfahrt, DLR) with funds provided by the Federal Ministry for Economic Affairs and Climate Action (Bundesministerium für Wirtschaft und Klimaschutz, BMWK) due to an enactment of the German Bundestag under Grant Nos. DLR 50WM1556, 50WM1641, 50WM1952, 50WM1956, 50WP1700, 50WM2250A-2250E (QUANTUS+),

50WM2450A-E (QUANTUS-VI), 50NA2106 (QGyro+), and 50WM2177-2178 (INTENTAS). D.S. gratefully acknowledges funding by the Federal Ministry of Education and Research (BMBF) through the funding program Photonics Research Germany under contract number 13N14875. E.G. thanks the German Research Foundation (Deutsche Forschungsgemeinschaft, DFG) for a Mercator Fellowship within CRC 1227 (DQ-mat). A.R. is supported by the Q-GRAV Project within the Space Research and Technology Program of the German Aerospace Center (DLR) W.P.S. is grateful to Texas A&M University for a Faculty Fellowship at the Hagler Institute of Advanced Study at Texas A&M University, and to Texas A&M AgriLife Research for the support of his work.

AUTHOR DECLARATIONS

Conflict of Interest

The authors have no conflicts to disclose.

Author Contributions

C. Schubert: Conceptualization (lead); Formal analysis (lead); Writing – original draft (equal); Writing – review & editing (equal). **D. Schlippert:** Formal analysis (supporting); Writing – review & editing (equal). **M. Gersemann:** Formal analysis (equal); Writing – review & editing (equal). **S. Abend:** Formal analysis (supporting); Writing – review & editing (equal). **E. Giese:** Formal analysis (equal); Writing – review & editing (equal). **A. Roura:** Formal analysis (supporting); Writing – review & editing (equal). **W. P. Schleich:** Writing – review & editing (equal). **W. Ertmer:** Writing – review & editing (equal). **E. M. Rasel:** Conceptualization (equal); Formal analysis (supporting); Supervision (lead); Writing – original draft (equal); Writing – review & editing (equal).

DATA AVAILABILITY

The data that support the findings of this study are available within the article.

APPENDIX A: PARAMETER ESTIMATE FOR TWIN-LATTICE AND RUBIDIUM

Initially, sequential double Bragg diffraction^{61,63,65,66} pulses couple the zero-momentum state to the $\pm 8 \hbar k_s$ momentum states where λ denotes the wavelength of the atomic transition and $k_s \equiv 2\pi/\lambda$ is the single-photon wave number. This momentum separation ensures an efficient transfer to higher momentum states with subsequent Bloch oscillations induced by counter-propagating lattices.⁶⁰ We expect a transfer of $1000 \hbar k_s$ differential momentum in 3 ms, leading to a total duration of 6 ms for a composite $\pi/2$ pulse. The two trajectories separate with a velocity of $\hbar k/m_{\text{Rb}} = 2000 \hbar k_s/m_{\text{Rb}}$ and are later deflected toward each other in a similar way in about 12 ms with $(5/4) \hbar k/m_{\text{Rb}} = 2500 \hbar k_s/m_{\text{Rb}}$ where m_{Rb} denotes the atomic mass of rubidium. Symmetric deceleration by Bloch lattices, sequential double Bragg π pulses, and symmetric acceleration by Bloch lattices invert the momentum.

In case of ⁸⁷Rb we have $\lambda = 780$ nm and the maximum wave packet separation would reach ~ 4.0 m.

The additional relaunch, required in the folded triple-loop interferometer, can be based on the same combination of Bloch lattices and double Bragg diffraction with a duration of 15 ms for the upward deflection.⁷⁰

APPENDIX B: COUPLING OF TIMING ERRORS AND COHERENT RELAUNCH

The differential measurement scheme of our detectors suppresses timing errors of the beam splitters to first order, because they are common to both atom interferometers contributing to the signal. On the contrary, the relaunches affect both atom interferometers individually. Relaunches that are not centered around the intersections of the trajectories induce a phase shift if in addition the projection of the relaunch vector onto the effective wave vector of the beam splitters is nonzero.

We estimate the impact on the detector by determining the mean trajectory of the atoms and subsequent calculation of the phase shift.⁷⁶ Here, we neglect rotations and gravity gradients which are discussed later on without timing errors.

Cutting the mean trajectory into sections, our set of equations reads

$$y_1(t) = y_0 + v_0 t \quad \text{for } t < t_1, \quad (\text{B1a})$$

$$y_2(t) = y_0 + v_0 t + \frac{\alpha_1 a_1}{2} (t_2 - t_1)^2 + \alpha_1 a_1 (t_2 - t_1)(t - t_2) \quad \text{for } t_2 < t < t_3, \quad (\text{B1b})$$

$$y_3(t) = y_0 + v_0 t + \frac{\alpha_1 a_1}{2} (t_2 - t_1)^2 + \alpha_1 a_1 (t_2 - t_1)(t_3 - t_2) + \frac{\alpha_2 a_2}{2} (t_4 - t_3)^2 + \alpha_2 a_2 (t_4 - t_3)(t - t_4) \quad \text{for } t_4 < t, \quad (\text{B1c})$$

with initial position y_0 , initial velocity v_0 , tilting angle deviation α_i from 90° with respect to the beam splitters, and acceleration during the relaunches a_i with $i = 1, 2$. Herein, t_1 marks the beginning of the first relaunch, t_2 its end, t_3 the beginning of the second relaunch, and t_4 its end, reflecting a finite duration of the relaunches.

The phase shift is estimated by

$$\phi = k \left[y_1(0) - \frac{9}{4} y_1(T) + \frac{5}{2} y_2(3T) - \frac{9}{4} y_3(5T) + y_3(6T) \right], \quad (\text{B2})$$

with the pulse separation time T and the effective wave number k , corresponding to the differential momentum between the two trajectories transferred during beam splitting.

We insert $t_1 = (9/5)T - (\tau_1/2) + \delta\tau_1$, $t_2 = (9/5)T + (\tau_1/2) + \delta\tau_1$, $t_3 = (21/5)T - (\tau_2/2) + \delta\tau_2$, $t_4 = (21/5)T + (\tau_2/2) + \delta\tau_2$ reflecting our interferometer. Here, $\tau_1 = t_2 - t_1$ and $\tau_2 = t_4 - t_3$ denote the durations of the respective relaunch pulses, displaced by $\delta\tau_1$ and $\delta\tau_2$ in time from the intersection of the trajectories.

Consequently, the phase shift simplifies to

$$\phi = \frac{5}{2} k (\alpha_2 a_2 \tau_2 \delta\tau_2 - \alpha_1 a_1 \tau_1 \delta\tau_1). \quad (\text{B3})$$

We use the definitions $\Sigma_\tau = \delta\tau_2 + \delta\tau_1$ and $\Delta\tau = \delta\tau_2 - \delta\tau_1$, assume equal duration $\tau_1 = \tau_2 = \tau$ and acceleration $a_1 = a_2 = a$ of the relaunches, to find the expression

$$\phi = \frac{5}{4}k \cdot a \cdot \tau \left(\Sigma_\tau \frac{\alpha_2 - \alpha_1}{2} + \Delta\tau \frac{\alpha_2 + \alpha_1}{2} \right). \quad (\text{B4})$$

According to the first term, a common timing error leads to a phase shift if a relative tilt between the relaunch vectors is present. For our parameters $k = 2000 \cdot 2\pi/(780 \text{ nm})$, $a \cdot \tau = (5/2)gT$, $T = 0.26 \text{ s}$, and $g = 9.81 \text{ m/s}^2$, this restricts a jitter in the differential angle $\Delta\alpha = \alpha_2 - \alpha_1$ to 1 nrad in 1 s for a common timing error Σ_τ of 10 ns to keep this contribution to the phase noise below 1 μrad in 1 s. The second term in Eq. (B4) appears in case of a differential timing error and a nonzero mean tilt. A differential timing error $\Delta\tau$ of 10 ns implies the restriction of a common tilt $\alpha_2 + \alpha_1$ to 1 nrad. Requirements on timings are within the capability of current real-time controllers. The common tilt can be adjusted with the interferometer itself by scanning the tilt angles for several differential timings $\Delta\tau$ while zeroing Σ_τ .

APPENDIX C: REQUIREMENTS IN A SINGLE-LOOP GEOMETRY

Gravity gradients, rotations, and other quantities can induce phase shifts in the differential signal of the two atom interferometers if the starting conditions are not matched. The estimation of phase terms to leading order^{75,76,125} in the limit of infinitely short pulses gives rise to the requirements for a single-loop interferometer summarized in Table II. Since some of these contributions intrinsically of higher order, the phase expressions listed in the table have to be seen as an order-of-magnitude estimate.

Ideally, instabilities in the starting conditions are shot-noise limited. Assuming that other noise contributions can be neglected, the instability of the mean position $r_m(n) = \sigma_r/\sqrt{n \cdot N}$ and velocity $v_m(n) = \sigma_v/\sqrt{n \cdot N}$ of the wave packet for n cycles depend on the number N of atoms per cycle, the initial radius σ_r , and expansion rate σ_v of the wave packet.

Gravity gradients Γ impose a limit on the instabilities of the center and the velocity of the wave packet to $4.3 \times 10^{-10} \text{ m}$ at 1 s and $1.7 \times 10^{-9} \text{ m/s}$ at 1 s, respectively, pointing instabilities of the initial launch to $\sim 10^{-9} \text{ rad}$ at 1 s, constraining initial radius and expansion rate of the wave packet to $4.3 \times 10^{-5} \text{ m}$ and $1.7 \times 10^{-4} \text{ m/s}$ for 10^{10} atoms per second, respectively. If the gravity gradients are equal and known at the two light-pulse atom interferometers interrogated by the same laser beam, an adjustment of the wave number at the second pulse can be introduced to relax these requirements.⁷⁹

Significantly more stringent conditions are set by the Sagnac effect caused by the rotation of the earth Ω which restricts instabilities in the pointing of the initial launch to the level of $2.2 \times 10^{-12} \text{ rad}$ at 1 s, and in the center of wave packet to $5.6 \times 10^{-12} \text{ m/s}$ at 1 s, implying a residual expansion rate of at most $5.6 \times 10^{-7} \text{ m/s}$ corresponding to few femtokelvins. The latter is challenging even for delta-kick collimated, dilute Bose-Einstein condensates.

Beam splitters which are not exactly perpendicular to gravity by an angle β induce a phase shift in a single interferometer that is suppressed in the differential signal. If the gravitational acceleration g differs at the locations of the two atom interferometers by δg , a spurious phase shift remains. Assuming $\delta g = 10^{-7}g$, instabilities in β have to be limited to 10^{-10} rad . A misalignment at the level of 10^{-10} rad implies less stringent requirements on initial radius and expansion of the wave packet than gravity gradients and rotations, even when assuming a compensation of gravity gradients⁷⁹ by a factor of 10^3 .

In addition, instabilities in density shifts $\propto \delta N/(\sigma_r)^3$ for an ensemble with N atoms and radius σ_r restrict the maximum initial density and fluctuations in the beam splitting fidelity δ which affects the relative density of atoms in the two arms.^{6,85} Assuming $\delta \sim 3 \times 10^{-5}$, a compensation of the phase shift induced by gravity

TABLE II. Phase shifts and requirements on key parameters of the atomic source and launch mechanism for the single-loop interferometer. The parameters in our estimation are: maximum phase noise of $\sigma_\phi = 1 \mu\text{rad}$ in 1 s, mean initial position $\delta y = r_{ip}(10)$, δr , mean initial velocities $\delta v_x = v_m(10) = \delta v_y$, $N = 10^9$ atoms injected every 0.1 s, $k = 2000 \cdot 2\pi/(780 \text{ nm})$, $T = 0.26 \text{ s}$, $\Gamma = 1.5 \times 10^{-6} \text{ 1/s}^2$, $\Omega = 5.75 \times 10^{-5} \text{ rad/s}$, gravitational acceleration $g = 9.81 \text{ m/s}^2$, distance between source and beam splitting zone $l = 30 \text{ cm}$, upward launch velocity gT , $\mathbf{k} \cdot \mathbf{g}/(|\mathbf{k}|g) \approx \beta$, difference in gravitational acceleration at the two atom interferometers $\delta g = 10^{-7}g$, angle between second and first beam splitter $\delta\beta_2$, angle between last and second beam splitter $\delta\beta_3$. Numerical values are given per second.

Parameter	Formula	Numerical value
Variation of mean position (y direction)	$\delta y = \sigma_\phi / (k\Gamma T^2 \cdot \sqrt{2})$	$\delta y = 4.3 \times 10^{-10} \text{ m}$
-Variation of launch angle (y direction)	$\delta\alpha_y = \sigma_\phi / (k\Gamma T^2 \cdot \sqrt{2} \cdot l)$	$\delta\alpha_y = 1.4 \times 10^{-9} \text{ rad}$
-Initial radius (y direction)	$\sigma_r = \delta y \cdot \sqrt{10 \cdot N}$	$\sigma_r = 4.3 \times 10^{-5} \text{ m}$
Variation of mean velocity (y direction)	$\delta v_y = \sigma_\phi / (k\Gamma T^3 \cdot \sqrt{2})$	$\delta v_y = 1.7 \times 10^{-9} \text{ m/s}$
-Variation of launch angle (y direction)	$\delta\alpha_{v,y} = \sigma_\phi / (k\Gamma T^3 \cdot \sqrt{2} \cdot gT)$	$\delta\alpha_{v,y} = 6.5 \times 10^{-10} \text{ rad}$
-Expansion rate (y direction)	$\sigma_v = \delta v_y \cdot \sqrt{10 \cdot N}$	$\sigma_v = 1.7 \times 10^{-4} \text{ m/s}$
Variation of mean velocity (x direction)	$\delta v_x = \sigma_\phi / (2k\Omega T^2 \cdot \sqrt{2})$	$\delta v_x = 5.6 \times 10^{-12} \text{ m/s}$
-Variation of launch angle (x direction)	$\delta\alpha_{v,x} = \sigma_\phi / (2k\Omega T^2 \cdot \sqrt{2} \cdot gT/2)$	$\delta\alpha_{v,x} = 2.2 \times 10^{-12} \text{ rad}$
-Expansion rate (x direction)	$\sigma_v = \delta v_x \cdot \sqrt{10 \cdot N}$	$\sigma_v = 5.6 \times 10^{-7} \text{ m/s}$
Difference in g, beam splitter pointing	$\sigma_\phi = k\delta g T^2 (\beta + \delta\beta_2 + \delta\beta_3)$	$\delta g = 10^{-7}g$, $\beta \approx \delta\beta_2 \approx \delta\beta_3 \approx 10^{-10} \text{ rad}$
Initial position, beam splitter pointing	$\sigma_\phi = k\delta r (-\delta\beta_2 + \delta\beta_3)$	$\delta r = 3.1 \times 10^{-7} \text{ m}$
-Initial radius	$\sigma_r = \delta r \cdot \sqrt{10 \cdot N}$	$\sigma_r = 9.8 \times 10^{-2} \text{ m}$
Initial velocity, beam splitter pointing	$\sigma_\phi = 2kT\delta v\delta\beta_3$	$\delta r = 8.4 \times 10^{-7} \text{ m/s}$
-Expansion rate	$\sigma_v = \delta v \cdot \sqrt{10 \cdot N}$	$\sigma_v = 2.7 \times 10^{-1} \text{ m/s}$

gradients⁷⁹ has to be implemented to at least a factor of 100 to simultaneously comply with the position requirement scaling as $\propto \sigma_r/\sqrt{N}$.

APPENDIX D: REQUIREMENTS IN A TRIPLE-LOOP GEOMETRY

Analogously to Appendix C, we rely on established methods^{46,75,76,125} to estimate phase terms to leading order for a triple-loop interferometer, deduce the requirements, and summarize them in Table III.

Compared to a single-loop arrangement, a coupling of the starting conditions to rotations and accelerations only appears in higher order terms, and leads to requirements which are relaxed by several orders of magnitude. Beam splitter tilts imply tighter bounds on the initial radius and expansion of the wave packet of 1.8×10^{-2} m and 1.6×10^{-2} m/s, still less stringent by orders of magnitude than for the single-loop geometry. Due to the modest requirement on the initial radius, the initial density can be adjusted to reduce the impact of interactions.^{6,85}

Pointing jitter of the relaunchees of the folded triple-loop geometry breaks the symmetry and leads to spurious phase shifts,

depending on gravity gradients and rotations. For our parameter set, rotations impose a limit on the jitter between the two subsequent relaunchees of 10^{-12} rad at 1 s.

APPENDIX E: DETECTOR ARRAY AND SIGNAL-TO-NOISE RATIO

Figure 3(a) shows spectral strain sensitivities over an extended frequency range, including estimations for the Einstein Telescope,²⁹ which targets a sensitivity around 10^{-21} Hz^{-1/2} at 1.5 Hz, as well as broad-band and resonant multi-loop interferometers in an array configuration.⁵⁹ For the array configuration we assume 80 pairs of atom interferometers in each arm of the gravitational wave detector with uncorrelated noise. Models project⁵⁹ that the specific spacing of these pairs on each arm may allow for the reduction of Newtonian noise by exploiting correlations.

Figure 3(b) shows the conversion of the estimates to characteristic strain.⁸⁷ We estimate a signal-to-noise ratio⁸⁷ of 2.3 for the broad-band multi-loop interferometer and 7 for broad-band multi-loop interferometer in array configuration for the depicted source⁴⁹ in Fig. 3.

TABLE III. Phase shifts and requirements on key parameters of the atomic source and launch mechanisms for the triple-loop interferometer. The angle between the two subsequent relaunchees is given by $\Delta\alpha$, the upward launch velocity by $gT/2$, variations $\delta\beta_i$ in the angle between the current beam splitter i and the previous one. Other parameters are the same as in Table II. Requirements on the mean position δy are less demanding than on the mean position δx .

Parameter	Formula	Numerical value
Relaunch pointing (y direction)	$\Delta\alpha = \sigma\phi/[-(39/10)k\Gamma gT^4 \cdot \sqrt{2}]$	$\Delta\alpha = 3.3 \times 10^{-10}$ rad
Relaunch pointing (x direction)	$\Delta\alpha = \sigma\phi/(9kgT^3\Omega \cdot \sqrt{2})$	$\Delta\alpha = 10^{-12}$ rad
Variation of mean position (y direction)	$\delta y = \sigma\phi/[(15/4)\Gamma^2 kT^4 \cdot \sqrt{2}]$	$\delta y = 1.1 \times 10^{-3}$ m
-Variation of launch angle (y direction)	$\delta\alpha_y = \sigma\phi/[(15/4)\Gamma^2 kT^4 \cdot \sqrt{2} \cdot l]$	$\delta\alpha_y = 3.8 \times 10^{-3}$ rad
-Initial radius (y direction)	$\sigma_r = \delta y \cdot \sqrt{10 \cdot N}$	$\sigma_r = 1.1 \times 10^2$ m
Variation of mean position (y direction)	$\delta y = \sigma\phi/[(45/4)kT^4 \cdot \sqrt{2}]$	$\delta y = 7.8 \times 10^1$ m
-Variation of launch angle (y direction)	$\delta\alpha_y = \sigma\phi/[(45/4)kT^4 \cdot \sqrt{2} \cdot l]$	$\delta\alpha_y = 2.6 \times 10^2$ rad
-Initial radius (y direction)	$\sigma_r = \delta y \cdot \sqrt{10 \cdot N}$	$\sigma_r = 7.8 \times 10^6$ m
Variation of mean velocity (y direction)	$\delta v_y = \sigma\phi/[(45/4)\Gamma^2 kT^5 \cdot \sqrt{2}]$	$\delta v_y = 1.5 \times 10^{-3}$ m/s
-Variation of launch angle (y direction)	$\delta\alpha_{v,y} = \sigma\phi/[(15\Gamma^2 kT^4 \cdot \sqrt{2} \cdot gT/2)]$	$\delta\alpha_{v,y} = 1.1 \times 10^{-3}$ rad
-Expansion rate (y direction)	$\sigma_v = \delta v_y \cdot \sqrt{10 \cdot N}$	$\sigma_v = 1.5 \times 10^2$ m/s
Variation of mean velocity (x direction)	$\delta v_x = \sigma\phi/(15kT^4\Omega^3 \cdot \sqrt{2})$	$\delta v_x = 3.4 \times 10^{-3}$ m/s
-Variation of launch angle (x direction)	$\delta\alpha_{v,x} = \sigma\phi/(15kT^4\Omega^3 \cdot \sqrt{2} \cdot gT/2)$	$\delta\alpha_{v,x} = 2.6 \times 10^{-3}$ rad
-Expansion rate (x direction)	$\sigma_v = \delta v_x \cdot \sqrt{10 \cdot N}$	$\sigma_v = 3.4 \times 10^2$ m/s
Variation of mean velocity (x direction)	$\delta v_x = \sigma\phi/[(15/4)\Gamma kT^4\Omega \cdot \sqrt{2}]$	$\delta v_x = 3 \times 10^{-5}$ m/s
-Variation of launch angle (x direction)	$\delta\alpha_{v,x} = \sigma\phi/[(15/4)\Gamma kT^4\Omega \cdot \sqrt{2} \cdot gT/2]$	$\delta\alpha_{v,x} = 2.3 \times 10^{-5}$ rad
-Expansion rate (x direction)	$\sigma_v = \delta v_x \cdot \sqrt{10 \cdot N}$	$\sigma_v = 3$ m/s
Difference in g, beam splitter pointing	$\sigma\phi = (9/8)k\delta gT^2(\delta\beta_3 - 9\delta\beta_4 + 16\delta\beta_5)$	$\delta g = 10^{-7} g$, $\delta\beta_3/16 = \delta\beta_4/9 = \delta\beta_5$ $= 4.8 \times 10^{-11}$ rad
Initial position, beam splitter pointing	$\sigma\phi = (1/4)k\delta r(-4\delta\beta_2 + 5\delta\beta_3 - 5\delta\beta_4 + 4\delta\beta_5)$	$\delta r = 1.8 \cdot 10^{-7}$ m, $(5/4)\delta\beta_2 = (5/4)\delta\beta_5$ $= \delta\beta_3 = \delta\beta_4 = 10^{-10}$ rad
-Initial radius	$\sigma_r = \delta r \cdot \sqrt{10 \cdot N}$	$\sigma_r = 1.8 \times 10^{-2}$ m
Initial velocity, beam splitter pointing	$\sigma\phi = (3/4)kT\delta v(3\delta\beta_3 - 7\delta\beta_4 - 8\delta\beta_5)$	$\delta v = 1.6 \times 10^{-7}$ m/s, $(3/8)\delta\beta_3 = (7/8)\delta\beta_4$ $= \delta\beta_5 = 10^{-10}$ rad
-Expansion rate	$\sigma_v = \delta v \cdot \sqrt{10 \cdot N}$	$\sigma_v = 1.6 \times 10^{-2}$ m

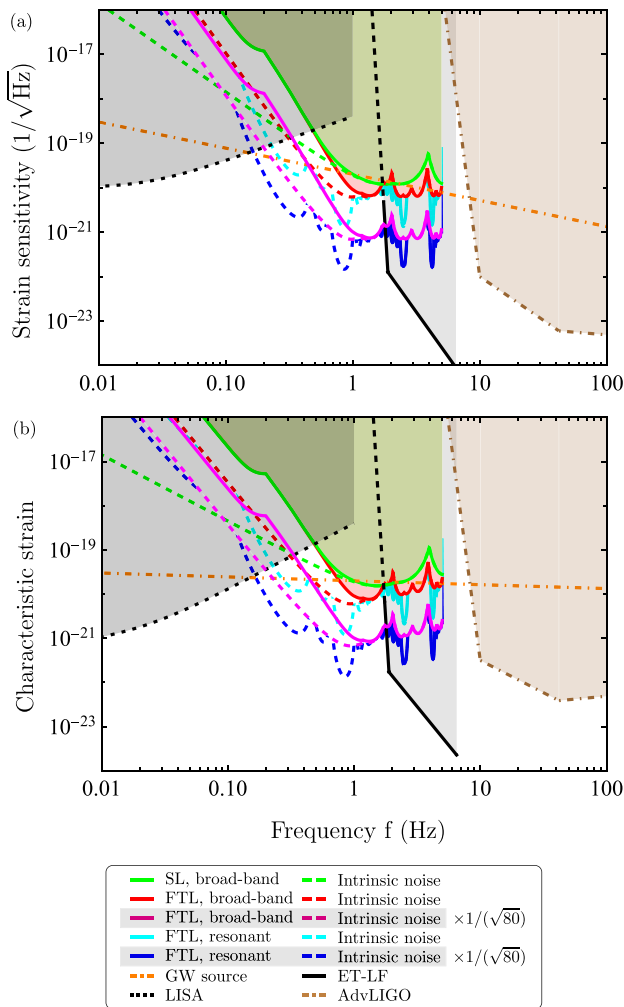


FIG. 3. Spectral strain sensitivities (a) and characteristic strain (b) of symmetric single- and multi-loop interferometers compared to broad-band (pink) and resonant multi-loop interferometers (blue) in an array configuration (Ref. 59) as well as the Einstein Telescope (black line, partially dashed) (Ref. 29). The array configuration assumes 80 pairs of atom interferometer in each arm of the gravitational wave detector and uncorrelated noise (Ref. 59). In addition, the strain induced by a black hole binary shown in Fig. 2 is also displayed.

REFERENCES

¹B. P. Abbott *et al.*, *Phys. Rev. Lett.* **116**, 061102 (2016).
²B. P. Abbott *et al.*, *Phys. Rev. Lett.* **116**, 221101 (2016).
³M. Abe, P. Adamson, M. Borcean, D. Bortoletto, K. Bridges, S. P. Carman, S. Chattopadhyay, J. Coleman, N. M. Curfman *et al.*, *Quantum Sci. Technol.* **6**, 044003 (2021).
⁴L. Badurina, E. Bentine, D. Blas, K. Bongs, D. Bortoletto, T. Bowcock, K. Bridges, W. Bowden, O. Buchmueller *et al.*, *J. Cosmol. Astropart. Phys.* **2020**, 011.
⁵B. Stray, O. Ennis, S. Hedges, S. Dey, M. Langlois, K. Bongs, S. Lellouch, M. Holynski, B. Bostwick *et al.*, *AVS Quantum Sci.* **6**, 014409 (2024).
⁶S. Dimopoulos, P. W. Graham, J. M. Hogan, and M. A. Kasevich, *Phys. Rev. D* **78**, 042003 (2008).
⁷J. Coleman *et al.*, “Matter-wave atomic gradiometer interferometric sensor (MAGIS-100) at Fermilab,” [arXiv:1812.00482](https://arxiv.org/abs/1812.00482) (2018).

⁸Q. Beaufils, L. A. Sidorenkov, P. Lebegue, B. Venon, D. Holleville, L. Volodimer, M. Lours, J. Junca, X. Zou *et al.*, *Sci. Rep.* **12**, 19000 (2022).
⁹See <https://magis.fnal.gov/> for “MAGIS-100, Atoms in free fall,” accessed 29 April 2024.
¹⁰M.-S. Zhan, J. Wang, W.-T. Ni, D.-F. Gao, G. Wang, L.-X. He, R.-B. Li, L. Zhou, X. Chen *et al.*, *Int. J. Mod. Phys. D* **29**, 1940005 (2020).
¹¹B. Canuel, S. Abend, P. Amaro-Seoane, F. Badaracco, Q. Beaufils, A. Bertoldi, K. Bongs, P. Bouyer, C. Braxmaier *et al.*, *Classical Quantum Gravity* **37**, 225017 (2020).
¹²B. Canuel, A. Bertoldi, L. Amand, E. Pozzo di Borgo, T. Chantrait, C. Danquigny, M. Dovale Álvarez, B. Fang, A. Freise *et al.*, *Sci. Rep.* **8**, 14064 (2018).
¹³S. Abend *et al.*, *AVS Quantum Sci.* **6**, 024701 (2024).
¹⁴P. W. Graham, J. M. Hogan, M. A. Kasevich, and S. Rajendran, *Phys. Rev. D* **94**, 104022 (2016).
¹⁵F. Di Pumpo, A. Friedrich, and E. Giese, *AVS Quantum Sci.* **6**, 014404 (2024).
¹⁶S.-w. Chiow and N. Yu, *Phys. Rev. D* **97**, 044043 (2018).
¹⁷M. Arca Sedda, C. P. L. Berry, K. Jani, P. Amaro-Seoane, P. Auclair, J. Baird, T. Baker, E. Berti, K. Breivik *et al.*, *Classical Quantum Gravity* **37**, 215011 (2020).
¹⁸F. Acernese *et al.*, *Classical Quantum Gravity* **32**, 024001 (2015).
¹⁹H. Grote, *Classical Quantum Gravity* **27**, 084003 (2010).
²⁰T. Robson, N. J. Cornish, and C. Liu, *Classical Quantum Gravity* **36**, 105011 (2019).
²¹P. Amaro-Seoane *et al.*, “Laser interferometer space antenna,” [arXiv:1702.00786](https://arxiv.org/abs/1702.00786) (2017).
²²P. Amaro-Seoane *et al.*, “The gravitational universe,” [arXiv:1305.5720](https://arxiv.org/abs/1305.5720) (2013).
²³P. Amaro-Seoane, S. Aoudia, S. Babak, P. Binétruy, E. Berti, A. Bohé, C. Caprini, M. Colpi, N. J. Cornish *et al.*, *Classical Quantum Gravity* **29**, 124016 (2012).
²⁴P. Auclair *et al.*, *Living Rev. Relativ.* **26**, 5 (2023).
²⁵K. A. Kuns, H. Yu, Y. Chen, and R. X. Adhikari, *Phys. Rev. D* **102**, 043001 (2020).
²⁶I. Mandel, A. Sesana, and A. Vecchio, *Classical Quantum Gravity* **35**, 054004 (2018).
²⁷S. Kawamura *et al.*, *Classical Quantum Gravity* **28**, 094011 (2011).
²⁸M. Punturo, M. Abernathy, F. Acernese, B. Allen, N. Andersson, K. Arun, F. Barone, B. Barr, M. Barsuglia *et al.*, *Classical Quantum Gravity* **27**, 194002 (2010).
²⁹X. Korovesi, L. Busch, E. Majorana, P. Puppò, P. Rapagnani, F. Ricci, P. Ruggi, and S. Grohmann, *Phys. Rev. D* **108**, 123009 (2023).
³⁰D. J. Reardon, A. Zic, R. M. Shannon, G. B. Hobbs, M. Bailes, V. D. Marco, A. Kapur, A. F. Rogers, E. Thrane *et al.*, *Astrophys. J. Lett.* **951**, L6 (2023).
³¹H. Xu, S. Chen, Y. Guo, J. Jiang, B. Wang, J. Xu, Z. Xue, R. N. Caballero, J. Yuan *et al.*, *Res. Astron. Astrophys.* **23**, 075024 (2023).
³²G. Agazie, A. Anumarlapudi, A. M. Archibald, Z. Arzoumanian, P. T. Baker, B. Bécsy, L. Blecha, A. Brazier, P. R. Brook *et al.*, *Astrophys. J. Lett.* **951**, L8 (2023).
³³J. Antoniadis, P. Arumugam, S. Arumugam, S. Babak, M. Bagchi, A.-S. Bak Nielsen, C. G. Bassa, A. Bathula, A. Berthreau *et al.*, *Astron. Astrophys.* **678**, A50 (2023).
³⁴O. D. Aguiar, *Res. Astron. Astrophys.* **11**, 1 (2011).
³⁵J. Weber, *Phys. Rev.* **117**, 306 (1960).
³⁶J. Weber, *Phys. Rev. Lett.* **22**, 1320 (1969).
³⁷Y. E. Nesterikhin, S. G. Rautian, and G. I. Smirnov, *Sov. Phys. JETP* **48**, 1 (1978), [*Zh. Eksp. Teor. Fiz.* **75**, 3 (1978)].
³⁸C. J. Bordé, J. Sharma, P. Tourrenc, and T. Damour, *J. Phys. Lett.* **44**, 983 (1983).
³⁹P. Tourrenc, T. Damour, J. Sharma, and C. J. Bordé, “Ultra-high laser spectroscopy of atoms as a probe of gravitational fields including gravitational radiation,” in *10th International Conference on General Relativity and Gravitation*, edited by B. Bertotti, F. de Felice, and N. A. Pascalon (Consiglio Nazionale delle Ricerche, Rome, 1983), Vol. 2, pp. 933–935.
⁴⁰W. P. Schleich, “Optische Tests der Allgemeinen Relativitätstheorie,” MPQ Report No. 89, 1984; W. P. Schleich and M. O. Scully, “Non-linear absorptions spectroscopy in an accelerated frame with application to gravity wave detection” (unpublished) (1984).

- ⁴¹Y. A. El-Neaj, C. Alpigiani, S. Amairi-Pyka, H. Araújo, A. Balaz, A. Bassi, L. Bathe-Peters, B. Battelier, A. Belić *et al.*, *EPJ Quantum Technol.* **7**, 6 (2020).
- ⁴²J. Ellis and V. Vaskonen, *Phys. Rev. D* **101**, 124013 (2020).
- ⁴³J. M. Hogan and M. A. Kasevich, *Phys. Rev. A* **94**, 033632 (2016).
- ⁴⁴P. W. Graham, J. M. Hogan, M. A. Kasevich, and S. Rajendran, *Phys. Rev. Lett.* **110**, 171102 (2013).
- ⁴⁵N. Yu and M. Tinto, *Gen. Relativ. Gravitation* **43**, 1943 (2011).
- ⁴⁶J. M. Hogan, D. M. S. Johnson, S. Dickerson, T. Kovachy, A. Sugarbaker, S-w Chiow, P. W. Graham, M. A. Kasevich, B. Saif *et al.*, *Gen. Relativ. Gravitation* **43**, 1953 (2011).
- ⁴⁷M. Hohensee, S.-Y. Lan, R. Houtz, C. Chan, B. Estey, G. Kim, P.-C. Kuan, and H. Müller, *Gen. Relativ. Gravitation* **43**, 1905 (2011).
- ⁴⁸S. Kolkowitz, I. Pikovski, N. Langellier, M. D. Lukin, R. L. Walsworth, and J. Ye, *Phys. Rev. D* **94**, 124043 (2016).
- ⁴⁹A. Sesana, *J. Phys.: Conf. Ser.* **840**, 012018 (2017).
- ⁵⁰C. Cutler and K. S. Thorne, “An overview of gravitational-wave sources,” in *General Relativity and Gravitation*, edited by N. T. Bishop and S. D. Maharaj (World Scientific, 2002), p. 72.
- ⁵¹P. W. Graham and S. Jung, *Phys. Rev. D* **97**, 024052 (2018).
- ⁵²B. P. Abbott *et al.*, *Astrophys. J. Lett.* **848**, L12 (2017).
- ⁵³Kindred concepts⁵⁵ were discussed for space-borne detectors.⁴⁶
- ⁵⁴B. Canuel, S. Abend, P. Amaro-Seoane, F. Badaracco, Q. Beauflis, A. Bertoldi, K. Bongs, P. Bouyer, C. Braxmaier *et al.*, “Technologies for the ELGAR large scale atom interferometer array,” [arXiv:2007.04014](https://arxiv.org/abs/2007.04014) (2020).
- ⁵⁵B. Dubetsky and M. A. Kasevich, *Phys. Rev. A* **74**, 023615 (2006).
- ⁵⁶A. Bertoldi, C.-H. Feng, D. S. Naik, B. Canuel, P. Bouyer, and M. Prevedelli, *Phys. Rev. Lett.* **127**, 013202 (2021).
- ⁵⁷C. Schubert, S. Abend, M. Gersemann, M. Gebbe, D. Schlipper, P. Berg, and E. M. Rasel, *Sci. Rep.* **11**, 16121 (2021).
- ⁵⁸J. Junca, A. Bertoldi, D. O. Sabulsky, G. Lefèvre, X. Zou, J.-B. Decitre, R. Geiger, A. Landragin, S. Gaffet *et al.*, *Phys. Rev. D* **99**, 104026 (2019).
- ⁵⁹W. Chaibi, R. Geiger, B. Canuel, A. Bertoldi, A. Landragin, and P. Bouyer, *Phys. Rev. D* **93**, 021101 (2016).
- ⁶⁰M. Gebbe, J.-N. Siemß, M. Gersemann, H. Müntinga, S. Herrmann, C. Lämmerzahl, H. Ahlers, N. Gaaloul, C. Schubert *et al.*, *Nat. Commun.* **12**, 2544 (2021).
- ⁶¹H. Ahlers, H. Müntinga, A. Wenzlawski, M. Krutzik, G. Tackmann, S. Abend, N. Gaaloul, E. Giese, A. Roura *et al.*, *Phys. Rev. Lett.* **116**, 173601 (2016).
- ⁶²T. Lévêque, A. Gauguet, F. Michaud, F. Pereira Dos Santos, and A. Landragin, *Phys. Rev. Lett.* **103**, 080405 (2009).
- ⁶³J. Küber, F. Schmaltz, and G. Birkel, “Experimental realization of double Bragg diffraction: robust beamsplitters, mirrors, and interferometers for Bose-Einstein condensates,” [arXiv:1603.08826](https://arxiv.org/abs/1603.08826) (2016).
- ⁶⁴M. J. Snadden, J. M. McGuirk, P. Bouyer, K. G. Haritos, and M. A. Kasevich, *Phys. Rev. Lett.* **81**, 971 (1998).
- ⁶⁵S. Hartmann, J. Jenewein, E. Giese, S. Abend, A. Roura, E. M. Rasel, and W. P. Schleich, *Phys. Rev. A* **101**, 053610 (2020).
- ⁶⁶E. Giese, A. Roura, G. Tackmann, E. M. Rasel, and W. P. Schleich, *Phys. Rev. A* **88**, 053608 (2013).
- ⁶⁷N. Malossi, Q. Bodart, S. Merlet, T. Lévêque, A. Landragin, and F. P. D. Santos, *Phys. Rev. A* **81**, 013617 (2010).
- ⁶⁸J. Jenewein, S. Hartmann, A. Roura, and E. Giese, *Phys. Rev. A* **105**, 063316 (2022).
- ⁶⁹R. Li, V. J. Martínez-Lahuerta, S. Seckmeyer, and N. G. K. Hammerer, “Robust double Bragg diffraction via detuning control,” [arXiv:2407.04754](https://arxiv.org/abs/2407.04754) (2024).
- ⁷⁰S. Abend, M. Gebbe, M. Gersemann, H. Ahlers, H. Müntinga, E. Giese, N. Gaaloul, C. Schubert, C. Lämmerzahl *et al.*, *Phys. Rev. Lett.* **117**, 203003 (2016).
- ⁷¹A. Bertoldi, F. Minardi, and M. Prevedelli, *Phys. Rev. A* **99**, 033619 (2019).
- ⁷²A. Bonnin, N. Zahzam, Y. Bidel, and A. Bresson, *Phys. Rev. A* **92**, 023626 (2015).
- ⁷³P. Cheinet, B. Canuel, F. Pereira Dos Santos, A. Gauguet, F. Yver-Leduc, and A. Landragin, *IEEE Trans. Instrum. Meas.* **57**, 1141 (2008).
- ⁷⁴C. Antoine, *Phys. Rev. A* **76**, 033609 (2007).
- ⁷⁵J. M. Hogan, D. M. S. Johnson, and M. A. Kasevich, “Light-pulse atom interferometry,” in *Atom Optics and Space Physics: Proceedings of the International School of Physics “Enrico Fermi,” Course CLXVIII*, edited by E. Arimondo, W. Ertmer, W. P. Schleich, and E. M. Rasel (IOS Press, 2009), p. 411.
- ⁷⁶C. J. Bordé, *Gen. Relativ. Gravitation* **36**, 475 (2004).
- ⁷⁷The nonzero duration of the atom-light interaction is neglected in the derivation of the phase terms since it does not qualitatively change the result.
- ⁷⁸A. Roura, W. Zeller, and W. P. Schleich, *New J. Phys.* **16**, 123012 (2014).
- ⁷⁹A. Roura, *Phys. Rev. Lett.* **118**, 160401 (2017).
- ⁸⁰J. Rudolph, *Dissertation* (Leibniz Universität Hannover, 2016).
- ⁸¹T. Kovachy, J. M. Hogan, A. Sugarbaker, S. M. Dickerson, C. A. Donnelly, C. Overstreet, and M. A. Kasevich, *Phys. Rev. Lett.* **114**, 143004 (2015).
- ⁸²H. Müntinga, H. Ahlers, M. Krutzik, A. Wenzlawski, S. Arnold, D. Becker, K. Bongs, H. Dittus, H. Duncker *et al.*, *Phys. Rev. Lett.* **110**, 093602 (2013).
- ⁸³C. Deppner, W. Herr, M. Cornelius, P. Stromberger, T. Sternke, C. Grzeschik, A. Grote, J. Rudolph, S. Herrmann *et al.*, *Phys. Rev. Lett.* **127**, 100401 (2021).
- ⁸⁴K.-P. Marzlin and J. Audretsch, *Phys. Rev. A* **53**, 312 (1996).
- ⁸⁵J. E. Debs, P. A. Altin, T. H. Barter, D. Döring, G. R. Dennis, G. McDonald, R. P. Anderson, J. D. Close, and N. P. Robins, *Phys. Rev. A* **84**, 033610 (2011).
- ⁸⁶B. P. Abbott *et al.*, *Phys. Rev. Lett.* **116**, 131103 (2016).
- ⁸⁷C. J. Moore, R. H. Cole, and C. P. L. Berry, *Classical Quantum Gravity* **32**, 015014 (2015).
- ⁸⁸O. Hosten, N. J. Engelsen, R. Krishnakumar, and M. A. Kasevich, *Nature* **529**, 505 (2016).
- ⁸⁹Z. Pagel, W. Zhong, R. H. Parker, C. T. Olund, N. Y. Yao, and H. Müller, *Phys. Rev. A* **102**, 053312 (2020).
- ⁹⁰M. Jaffe, V. Xu, P. Haslinger, H. Müller, and P. Hamilton, *Phys. Rev. Lett.* **121**, 040402 (2018).
- ⁹¹B. Plotkin-Swing, D. Gochnauer, K. E. McAlpine, E. S. Cooper, A. O. Jamison, and S. Gupta, *Phys. Rev. Lett.* **121**, 133201 (2018).
- ⁹²T. Kovachy, P. Asenbaum, C. Overstreet, C. A. Donnelly, S. M. Dickerson, A. Sugarbaker, J. M. Hogan, and M. A. Kasevich, *Nature* **528**, 530 (2015).
- ⁹³G. D. McDonald, C. C. N. Kuhn, S. Bennetts, J. E. Debs, K. S. Hardman, J. D. Close, and N. P. Robins, *Europhys. Lett.* **105**, 63001 (2014).
- ⁹⁴S.-w. Chiow, T. Kovachy, H.-C. Chien, and M. A. Kasevich, *Phys. Rev. Lett.* **107**, 130403 (2011).
- ⁹⁵H. Müller, S.-w. Chiow, S. Herrmann, and S. Chu, *Phys. Rev. Lett.* **102**, 240403 (2009).
- ⁹⁶P. Cladé, S. Guellati-Khélifa, F. Nez, and F. Biraben, *Phys. Rev. Lett.* **102**, 240402 (2009).
- ⁹⁷S. S. Szigeti, J. E. Debs, J. J. Hope, N. P. Robins, and J. D. Close, *New J. Phys.* **14**, 023009 (2012).
- ⁹⁸A. Béguin, T. Rodzinka, L. Calmels, B. Allard, and A. Gauguet, *Phys. Rev. Lett.* **131**, 143401 (2023).
- ⁹⁹D. O. Sabulsky, J. Junca, X. Zou, A. Bertoldi, M. Prevedelli, Q. Beauflis, R. Geiger, A. Landragin, P. Bouyer *et al.*, *Phys. Rev. Lett.* **132**, 213601 (2024).
- ¹⁰⁰T. Rodzinka, E. Dionis, L. Calmels, S. Beldjoudi, A. Béguin, D. Guéry-Odelin, B. Allard, D. Sugny, and A. Gauguet, “Optimal Floquet engineering for large scale atom interferometers,” [arXiv:2403.14337](https://arxiv.org/abs/2403.14337) (2024).
- ¹⁰¹K. J. Hughes, J. H. T. Burke, and C. A. Sackett, *Phys. Rev. Lett.* **102**, 150403 (2009).
- ¹⁰²J. Glick, Z. Chen, T. Deshpande, Y. Wang, and T. Kovachy, *AVS Quantum Sci.* **6**, 014402 (2024).
- ¹⁰³S. M. Dickerson, J. M. Hogan, A. Sugarbaker, D. M. S. Johnson, and M. A. Kasevich, *Phys. Rev. Lett.* **111**, 083001 (2013).
- ¹⁰⁴L. Morel, Z. Yao, P. Cladé, and S. Guellati-Khélifa, *Nature* **588**, 61 (2020).
- ¹⁰⁵G. Louie, Z. Chen, T. Deshpande, and T. Kovachy, *New J. Phys.* **25**, 083017 (2023).
- ¹⁰⁶J. C. Saywell, M. S. Carey, P. S. Light, S. S. Szigeti, A. R. Milne, K. S. Gill, M. L. Goh, V. S. Perunicic, N. M. Wilson *et al.*, *Nat. Commun.* **14**, 7626 (2023).
- ¹⁰⁷M. H. Goerz, M. A. Kasevich, and V. S. Malinovsky, *Atoms* **11**, 36 (2023).
- ¹⁰⁸F. Anders, A. Idel, P. Feldmann, D. Bondarenko, S. Loriani, K. Lange, J. Peise, M. Gersemann, B. Meyer-Hoppe *et al.*, *Phys. Rev. Lett.* **127**, 140402 (2021).
- ¹⁰⁹I. Kruse, K. Lange, J. Peise, B. Lücke, L. Pezzè, J. Arlt, W. Ertmer, C. Lisdat, L. Santos *et al.*, *Phys. Rev. Lett.* **117**, 143004 (2016).
- ¹¹⁰L. Salvi, N. Poli, V. Vuletić, and G. M. Tino, *Phys. Rev. Lett.* **120**, 033601 (2018).
- ¹¹¹G. P. Greve, C. Luo, B. Wu, and J. K. Thompson, *Nature* **610**, 472 (2022).
- ¹¹²D. Savoie, M. Altorio, B. Fang, L. A. Sidorenkov, R. Geiger, and A. Landragin, *Sci. Adv.* **4**, eaau7948 (2018).

- ¹¹³I. Dutta, D. Savoie, B. Fang, B. Venon, C. L. Garrido Alzar, R. Geiger, and A. Landragin, *Phys. Rev. Lett.* **116**, 183003 (2016).
- ¹¹⁴M. Gebbe, "Atom interferometry in a twin lattice," *Dissertation* (Universität Bremen, 2020).
- ¹¹⁵H. J. Landau, *Proc. IEEE* **55**, 1701 (1967).
- ¹¹⁶S. Dimopoulos, P. W. Graham, J. M. Hogan, M. A. Kasevich, and S. Rajendran, *Phys. Rev. D* **78**, 122002 (2008).
- ¹¹⁷G. Losurdo, M. Bernardini, S. Braccini, C. Bradaschia, C. Casciano, V. Dattilo, R. De Salvo, A. Di Virgilio, F. Frasconi *et al.*, *Rev. Sci. Instrum.* **70**, 2507 (1999).
- ¹¹⁸J. Mitchell, T. Kovachy, S. Hahn, P. Adamson, and S. Chattopadhyay, *J. Inst.* **17**, P01007 (2022).
- ¹¹⁹J. Harms, B. J. J. Slagmolen, R. X. Adhikari, M. C. Miller, M. Evans, Y. Chen, H. Müller, and M. Ando, *Phys. Rev. D* **88**, 122003 (2013).
- ¹²⁰P. R. Saulson, *Phys. Rev. D* **30**, 732 (1984).
- ¹²¹J. Liu, L. Ju, and D. G. Blair, *Phys. Lett. A* **228**, 243 (1997).
- ¹²²K. U. Schreiber, T. Klügel, J.-P. R. Wells, R. B. Hurst, and A. Gebauer, *Phys. Rev. Lett.* **107**, 173904 (2011).
- ¹²³M. Meunier, I. Dutta, R. Geiger, C. Guerlin, C. L. Garrido Alzar, and A. Landragin, *Phys. Rev. A* **90**, 063633 (2014).
- ¹²⁴G. W. Biedermann, K. Takase, X. Wu, L. Deslauriers, S. Roy, and M. A. Kasevich, *Phys. Rev. Lett.* **111**, 170802 (2013).
- ¹²⁵K. Bongs, R. Launay, and M. Kasevich, *Appl. Phys. B* **84**, 599 (2006).